inorganics

MDPI

Article

Synthesis, X-ray Structure of Two Hexa-Coordinated Ni(II) Complexes with *s*-Triazine Hydrazine Schiff Base Ligand

Eman M. Fathalla [1,*], Morsy A. M. Abu-Youssef [1,*], Mona M. Sharaf [2], Ayman El-Faham [1], Assem Barakat [3], Matti Haukka [4] and Saied M. Soliman [1,*]

[1] Department of Chemistry, Faculty of Science, Alexandria University, P.O. Box 426, Ibrahimia, Alexandria 21321, Egypt; ayman.elfaham@alexu.edu.eg or aymanel_faham@hotmail.com
[2] Protein Research Department, Genetic Engineering and Biotechnology Research Institute, City of Scientific Research and Technological Applications, Alexandria, P.O. Box 21933, Egypt; sharafmona4@gmail.com
[3] Department of Chemistry, College of Science, King Saud University, P.O. Box 2455, Riyadh 11451, Saudi Arabia; ambarakat@ksu.edu.sa
[4] Department of Chemistry, University of Jyväskylä, P.O. Box 35, FI-40014 Jyväskylä, Finland; matti.o.haukka@jyu.fi
* Correspondence: eman.nomeir@alexu.edu.eg (E.M.F.); morsy5@alexu.edu.eg (M.A.M.A.-Y.); saied1soliman@yahoo.com or saeed.soliman@alexu.edu.eg (S.M.S.)

Abstract: The hydrazine *s*-triazine ligand (*E*)-4,4′-(6-(2-(1-(pyridin-2-yl)ethylidene)hydrazinyl)-1,3,5-triazine-2,4-diyl)dimorpholine (DMPT) was used to synthesize two new Ni(II) complexes via a self-assembly technique. The two complexes were synthesized by a one-pot synthesis strategy and characterized by elemental analysis, FTIR and single-crystal X-ray diffraction analysis to be $[Ni(DMPT)(H_2O)_3](NO_3)_2.3H_2O$ (**1**) and $[Ni(DMPT)(H_2O)_3](NO_3)_2.H_2O$ (**2**). The structures of both complexes were very similar regarding the coordination sphere and counter anions, but differ only in the number of the crystal water molecules. In the case of complex **1**, there are three water molecules instead of one H_2O molecule as in complex **2**. In the two complexes, the DMPT ligand acts as a neutral tridentate *NNN*-chelate via three Ni–N coordination interactions. The coordination sphere of the Ni(II) ion is completed by three water molecules. As a result, the two complexes exhibit distorted octahedral geometry. The Hirshfeld surfaces around each entity in both complexes have been computed. Subsequently, their corresponding intermolecular interactions were quantified separately. Because the number of crystal water molecules is different in both complexes, their monomeric units are connected differently in their crystal structures where the crystal water molecules act as both hydrogen bond donor and acceptor. The polar O . . . H interactions are the most dominant in all entities of both complexes. As a result, strong O . . . H interactions are the driving force in the crystal packing of both complexes, and this is attributed to the presence of the nitrate anions and water molecules. The antimicrobial activity of the free ligand and complex **1** were determined against two selected fungal species, Gram-negative and Gram-positive bacterial strains. The free ligand was found to be inactive against all microbial species. On the other hand, the Ni(II) complex **1** was found active against the Gram-positive bacterial species *Bacillus subtilis* and also the Gram-negative bacterial species *Escherichia coli*. The respective inhibition zone diameter of the Ni(II) complex was 12 and 11 mm, respectively.

Keywords: *s*-triazine hydrazone; molecular packing; X-ray; Ni(II) complexes; Hirshfeld surface; antimicrobial

Citation: Fathalla, E.M.; Abu-Youssef, M.A.M.; Sharaf, M.M.; El-Faham, A.; Barakat, A.; Haukka, M.; Soliman, S.M. Synthesis, X-ray Structure of Two Hexa-Coordinated Ni(II) Complexes with *s*-Triazine Hydrazine Schiff Base Ligand. *Inorganics* **2023**, *11*, 222. https://doi.org/10.3390/inorganics11050222

Academic Editors: Wolfgang Linert, Gabriel García Sánchez, David Turner and Koichiro Takao

Received: 9 May 2023
Revised: 19 May 2023
Accepted: 19 May 2023
Published: 21 May 2023

1. Introduction

Schiff base ligands are an important class of organic chelating ligands which have been widely used for the synthesis of a large number of metal complexes. Schiff bases have become a significant class of ligands that are widely used in coordination chemistry and are considered as privileged multitopic ligands. There is a wide range of potential uses for

Schiff bases and their metal complexes, including luminescent probes [1], catalysis [2–5], dye and polymer industry, analytical chemistry, agriculture [6–8], magneto-structural chemistry, food industry, agrochemical and biological fields [9,10], and also as antitumor, antifungal and antimicrobial agents [11–22]. Hydrazones Schiff bases are among these important chelating ligands which have drawn particular interest from researchers because of their known chelating ability beside their structural flexibility, which can add stiffness to the skeletal structure of the synthesized metal complexes [23–27]. In addition, the nitrogen–nitrogen covalent bond that exists in the azomethine group of hydrazones increases its ability to synthesize stable metal complexes. Additionally, hydrazones and related compounds play a significant part in enhancing the toxicity and selectivity aspects of some anticancer agents by building drug carrier systems using proper carrier proteins [28].

On the other hand, the majority of the first row of transition metals and their complexes have biological necessities and a variety of known bioactivities. One of these transition metals is nickel, which exists in the nickel (II) form as the most stable oxidation state [29–31]. Ni(II) complexes are one of these crucial transition metal complexes which have different coordination geometries, including tetrahedral [32], square planar [32,33], trigonal bipyramidal [34] and octahedral [35], where the square planar and octahedral geometries are the most prevalent. Each nickel (II) complex with a particular ligand has unique chemical and physical characteristics, which makes their investigation both fascinating and challenging. Its significance in bioinorganic chemistry expands with the identification of the nickel enzyme, urease [36,37]. The ability of nickel complexes to permeate into the microbial cells and impact the enzyme activity has led to the discovery of numerous nickel complexes with broad-spectrum efficacy against many pathogens [38–44].

In our previous work, the X-ray structure and biological evaluations of the three metal complexes, [Mn(DMPT)Cl_2], [Cu(DMPT)Cl_2]. H_2O and [Cu(DMPT)$(NO_3)_2$] were presented. In continuation to our previous study, the present work aims to synthesize two novel Ni(II) complexes using the hydrazine *s*-triazine ligand DMPT [45] shown in Figure 1. The synthesized complexes were characterized by different analytical techniques such as FTIR, single-crystal X-ray diffraction (SCXRD) and elemental analysis. Hirshfeld surface analysis is performed to describe and quantify the intermolecular interactions in their crystal structures. Additionally, an assessment of their antibacterial activity against six harmful microorganisms was performed.

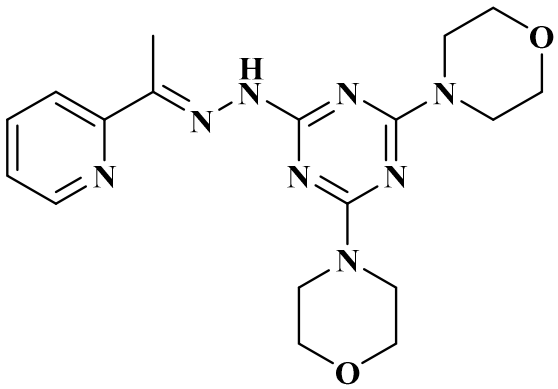

Figure 1. Structure of DMPT.

2. Results and Discussion

2.1. Synthesis and Characterizations

The self-assembly of the organic ligand (DMPT) [45] and $Ni(NO_3)_2.6H_2O$ in ethanol lead to the formation of two new crystalline Ni(II) complexes in the same pot (Scheme 1). The two complexes **1** and **2** were distinguished very clearly as green and turquoise crystals, respectively. Additionally, both complexes are separated easily from the reaction pot as the green crystals of **1** were formed on the glass beaker's walls, while turquoise crystals of **2** were collected from the bottom of the beaker. FTIR data of the ligand DMPT and its

two complexes were compared in Figure S1 (Supplementary Data). The FTIR spectra of DMPT showed the ν(C=N) modes at 1523 and 1492 cm^{-1}. These bands are shifted to higher wavenumbers of 1593 and 1572 cm^{-1} in the case of **1**, while appeared as a split band at 1575 and 1607 cm^{-1} in the case of **2**, indicating the coordination of the Ni(II) ion in the two complexes via the nitrogen atoms of azomethine, triazine and pyridine moieties of DMPT. The broad band at 3382 cm^{-1} in complex **1** and 3327 cm^{-1} in complex **2** confirms the presence of water molecules in the two complexes. Additionally, the (N–O) stretches of the nitrate group in the two complexes appeared at the same frequency at 1385 cm^{-1}.

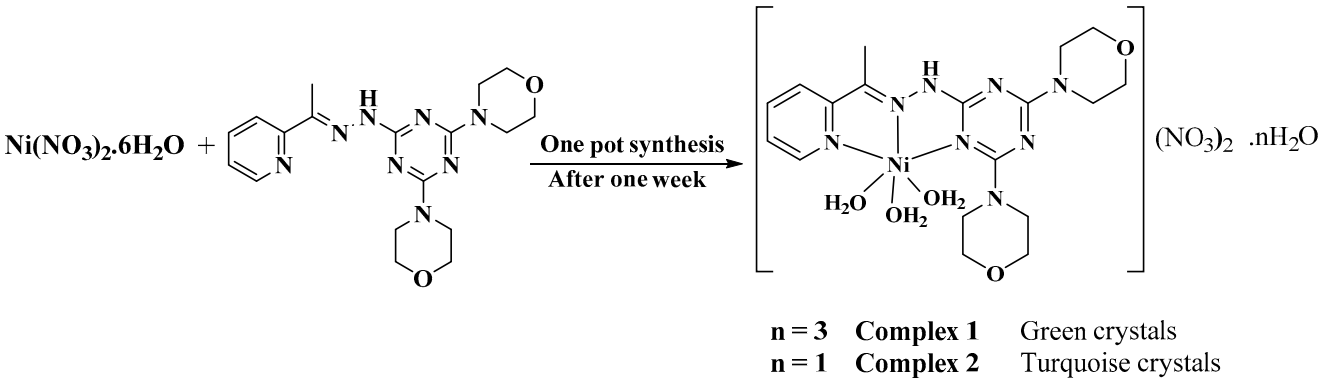

Scheme 1. Synthesis of complexes **1** and **2**.

2.2. X-ray Structure Description

The molecular structure of complex **1** was confirmed by crystal X-ray diffraction to be $[Ni(DMPT)(H_2O)_3](NO_3)_2.3H_2O$. The crystal system of **1** is monoclinic and the space group is $P2_1/n$. The unit cell parameters are a = 11.4900(2) Å, b = 17.6794(3) Å, c = 14.1294(2) Åand β = 90.110(1)°. In the unit cell, there are four molecules of the abovementioned formula and its volume is 2870.19(8) $Å^3$, while the calculated density is 1.563 mg/m^3. The asymmetric formula is one $[Ni(DMPT)(H_2O)_3](NO_3)_2.3H_2O$ molecule (Figure 2).

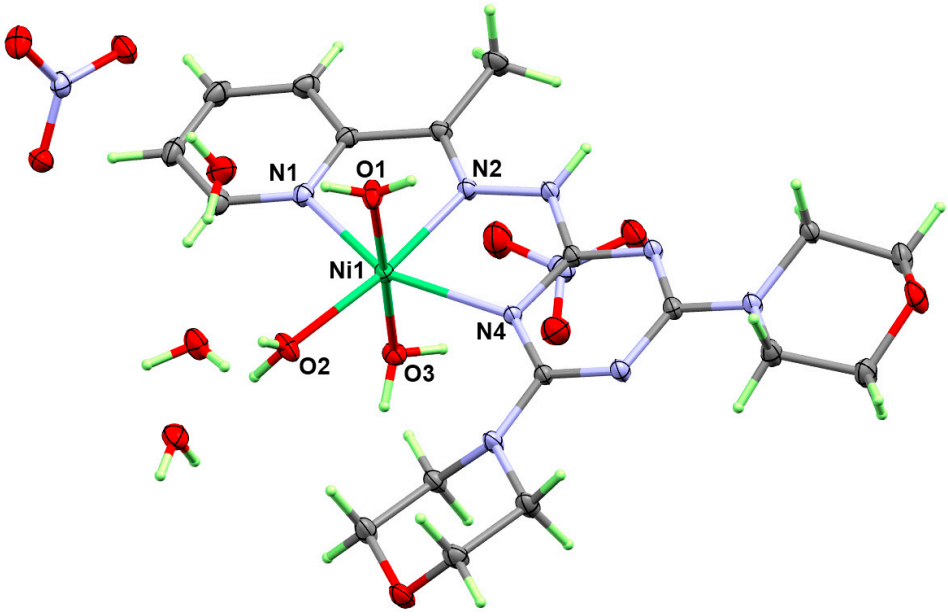

Figure 2. Asymmetric unit of $[Ni(DMPT)(H_2O)_3](NO_3)_2.3H_2O$ (**1**).

The inner sphere of this complex comprised a hexa-coordinated Ni(II) ion with one DMPT and three water molecules, while the outer sphere composed of two nitrate counter ions and three crystal water molecules. It is clear from Figure 2 that the DMPT ligand acts

as a neutral tridentate *NNN*-chelate via three Ni–N coordination interactions which are the Ni(1)–N(2), Ni(1)–N(1) and Ni(1)–N(4) bonds. Their respective Ni–N distances are 2.0031(12), 2.1002(13) and 2.2608(12) Å, respectively. It is clear that the Ni–$N_{(hydrazone)}$ is the shortest interaction. In contrast, the Ni–$N_{(s\text{-triazine})}$ is the longest Ni–N bond. The chelate angles N(2)–Ni(1)–N(1) and N(2)–Ni(1)–N(4) are determined to be 77.93(5) and 76.47(4)°, respectively, while the trans-N(1)–Ni(1)–N(4) is determined to be 154.38(5)°. On the other hand, the coordination sphere of the Ni(II) ion is completed by three water molecules. The equatorial Ni1–O2 bond, which is trans to the Ni–$N_{(hydrazone)}$ bond, is the shortest interaction with the water molecules. The two axial Ni1–O3 and Ni1–O4 bonds are slightly longer than the equatorial Ni–O bond. The corresponding Ni–O distances are 2.0466(12) and 2.0764(12) Å, respectively (Table 1). The distorted octahedron comprised the four atoms N1, N2, N4 and O2 as corners for the distorted square as a basal plane, while the two oxygens O1 and O3 are apical.

Table 1. Bond distances and angles (Åand °) for the coordination environment of $[Ni(DMPT)(H_2O)_3](NO_3)_2.3H_2O$ complex.

Bond	**Distance**	**Bond**	**Distance**
Ni(1)–N(2)	2.0031(12)	Ni(1)–O(3)	2.0764(12)
Ni(1)–O(2)	2.0242(12)	Ni(1)–N(1)	2.1002(13)
Ni(1)–O(1)	2.0466(12)	Ni(1)–N(4)	2.2608(12)
Bonds	**Angle**	**Bonds**	**Angle**
N(2)–Ni(1)–O(2)	171.68(5)	O(1)–Ni(1)–N(1)	92.93(5)
N(2)–Ni(1)–O(1)	90.08(5)	O(3)–Ni(1)–N(1)	87.39(5)
O(2)–Ni(1)–O(1)	90.28(5)	N(2)–Ni(1)–N(4)	76.47(4)
N(2)–Ni(1)–O(3)	91.46(5)	O(2)–Ni(1)–N(4)	111.85(5)
O(2)–Ni(1)–O(3)	88.20(5)	O(1)–Ni(1)–N(4)	88.12(5)
O(1)–Ni(1)–O(3)	178.46(5)	O(3)–Ni(1)–N(4)	92.24(5)
N(2)–Ni(1)–N(1)	77.93(5)	N(1)–Ni(1)–N(4)	154.38(5)
O(2)–Ni(1)–N(1)	93.75(5)		

As clearly seen from Figure 2, the solid state structure of complex **1** comprised a large number of coordinated and hydration water molecules which participate significantly with the nitrate counter anions in the molecular packing of this monomeric complex. The important hydrogen bond contacts are shown in Figure 3A and the corresponding geometric parameters are depicted in Table 2. The nitrate counter ions as hydrogen bond acceptor connect the monomeric complex units via short hydrogen bonding interactions with the free and coordinated water molecules. In this supramolecular structure, the free water molecules act as both hydrogen bond donors as well as hydrogen bond acceptors while the coordinated H_2O molecules are only hydrogen bond donors. In addition, the oxygen atom of the morpholine substituents and one of the free triazine N-atoms (N5) participated in the molecular packing of complex **1** as hydrogen bond acceptors (Figure 3B).

On the other hand, the structure of complex **2** was found very similar to that for **1** regarding the coordination sphere and counter anions but differ only in the number of the crystal water molecules. In case of complex **2**, there is one water molecule instead of three H_2O molecules in complex **1**. Additionally, this complex crystallized in the less symmetric triclinic crystal system and *P-1* space group. The unit cell parameters are a = 8.3135(2) Å, b = 10.9175(2) Å, c = 15.7611(4) Å, α = 71.119(1)°, β = 80.188(1)° and γ = 84.58(1)°. In the unit cell there are two molecules of the asymmetric formula $[Ni(DMPT)(H_2O)_3](NO_3)_2.H_2O$ and its volume is 1332.20(5) $Å^3$ while the calculated density is 1.594 mg/m^3 (Figure 4).

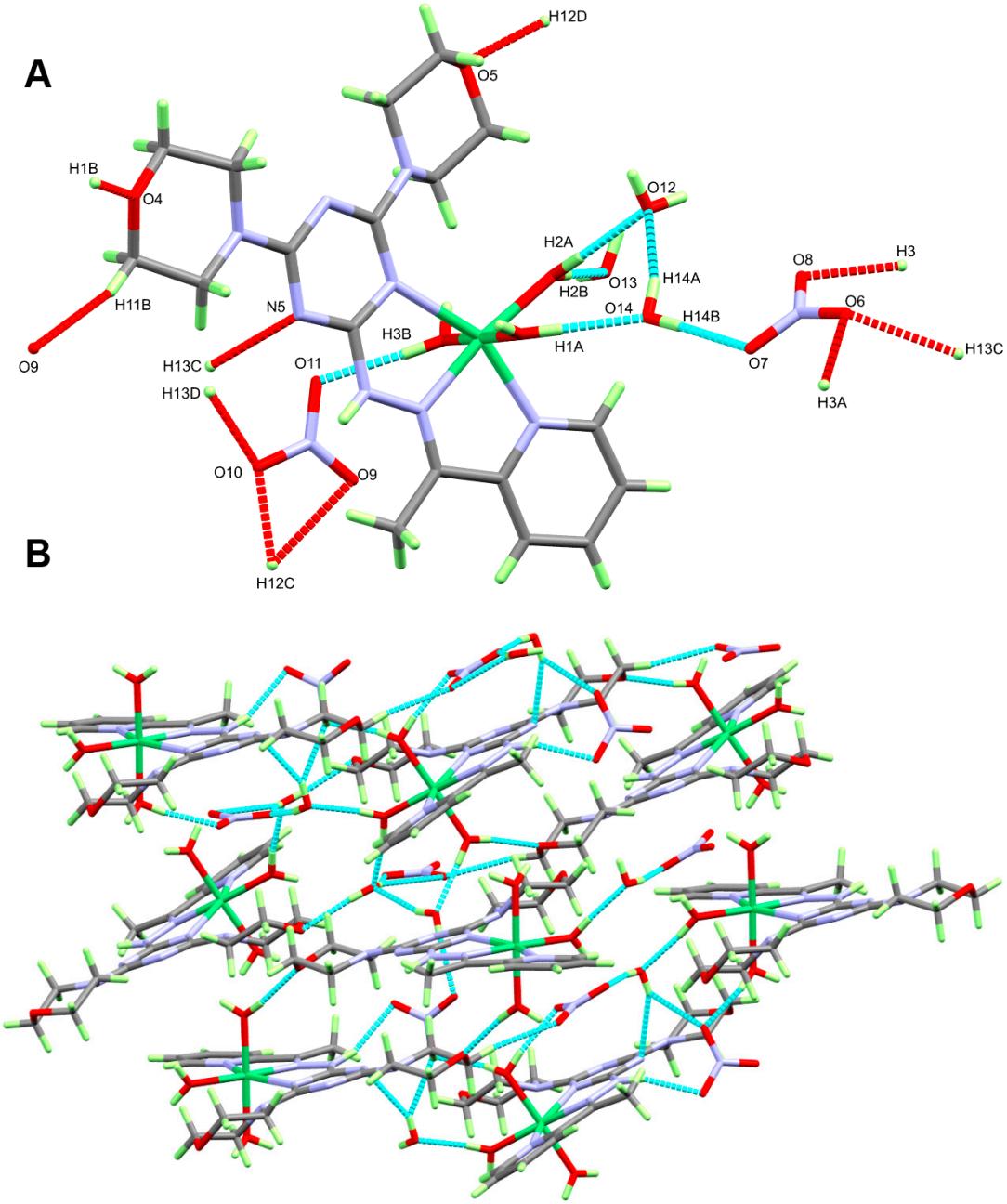

Figure 3. All of the important hydrogen bond contacts (**A**) and 3D H-bonding network (**B**) in $[Ni(DMPT)(H_2O)_3](NO_3)_2.3H_2O$ complex.

The structure of the coordination sphere of complex **2** comprised one tridentate DMPT molecule and three water molecules. Similar to complex **1**, the $Ni–N_{(hydrazone)}$ bond is the shortest Ni–N interaction with the organic ligand compared to the $Ni–N_{(s\text{-}triazine)}$ and $Ni–N_{(pyridine)}$ bonds. The respective Ni–N distances are 2.0079(18) Å, 2.1031(18) and 2.1907(18) Å. The N(2)–Ni(1)–N(1) and N(2)–Ni(1)–N(8) angles are 78.11(7) and 77.95(7)°, respectively, while the trans N(1)–Ni(1)–N(8) is 156.03(7)°. The hexa-coordination environment of the Ni(II) is completed by the three Ni(1)–O(2), Ni(1)–O(3) and Ni(1)–O(1) bonds. The respective Ni–O distances are 2.0378(17), 2.0409(17) and 2.0652(16) Å, respectively (Table 3). Additionally, the equatorial Ni1–O2 bond is the shortest Ni–O bonds. The results of these geometric parameters are similar to those for complex **1** and the NiN_3O_3 coordination environment of the Ni(II) ion could be described as a distorted octahedron.

Table 2. The hydrogen bond geometric parameters in $[Ni(DMPT)(H_2O)_3](NO_3)_2.3H_2O$.

D–H . . . A	D–H/Å	H . . . A/Å	D . . . A/Å	D–H . . . A/°	Symm. Code
C(11)–H(11B)...O(9)#1	0.99	2.39	3.356(2)	165.2	#1 −x + 3/2, y + 1/2, −z + 1/2
N(3)–H(3)...O(8)#2	0.88(2)	2.07(2)	2.9043(18)	158.0(19)	#2 −x + 1/2, y + 1/2, −z + 1/2
O(1)–H(1A)...O(14)	0.82(2)	1.82(2)	2.6391(19)	179(2)	
O(3)–H(3A)...O(6)#3	0.83(3)	2.00(3)	2.8245(18)	170(2)	#3 x + 1, y, z
O(12)–H(12C)...O(9)#4	0.84(3)	2.46(3)	3.091(2)	133(2)	#4 x − 1/2, −y + 1/2, z + 1/2
O(12)–H(12C)...O(10)#4	0.84(3)	2.04(3)	2.870(2)	170(3)	#4 x − 1/2, −y + 1/2, z + 1/2
O(12)–H(12D)...O(5)#5	0.83(3)	1.98(3)	2.7972(17)	169(2)	#5 −x + 1, −y, −z + 1
O(3)–H(3B)...O(11)	0.85(2)	1.91(2)	2.7540(18)	171(2)	
O(13)–H(13C)...N(5)#6	0.80(3)	2.41(3)	3.138(2)	152(2)	#6 −x + 3/2, y − 1/2, −z + 1/2
O(13)–H(13C)...O(6)#3	0.80(3)	2.43(3)	2.9541(19)	124(2)	#3 x + 1, y, z
O(14)–H(14A)...O(12)	0.81(3)	1.96(3)	2.730(2)	159(3)	
O(2)–H(2A)...O(12)	0.80(3)	1.93(3)	2.7227(18)	171(3)	
O(2)–H(2B)...O(13)	0.84(3)	1.85(3)	2.6901(18)	175(2)	
O(1)–H(1B)...O(4)#7	0.82(3)	1.95(3)	2.7684(17)	171(3)	#7 −x + 1, −y + 1, −z + 1
O(14)–H(14B)...O(7)	0.81(3)	2.01(3)	2.810(2)	176(3)	
O(13)–H(13D)...O(10)#6	0.83(3)	2.05(3)	2.861(2)	165(3)	#6 −x + 3/2, y − 1/2, −z + 1/2

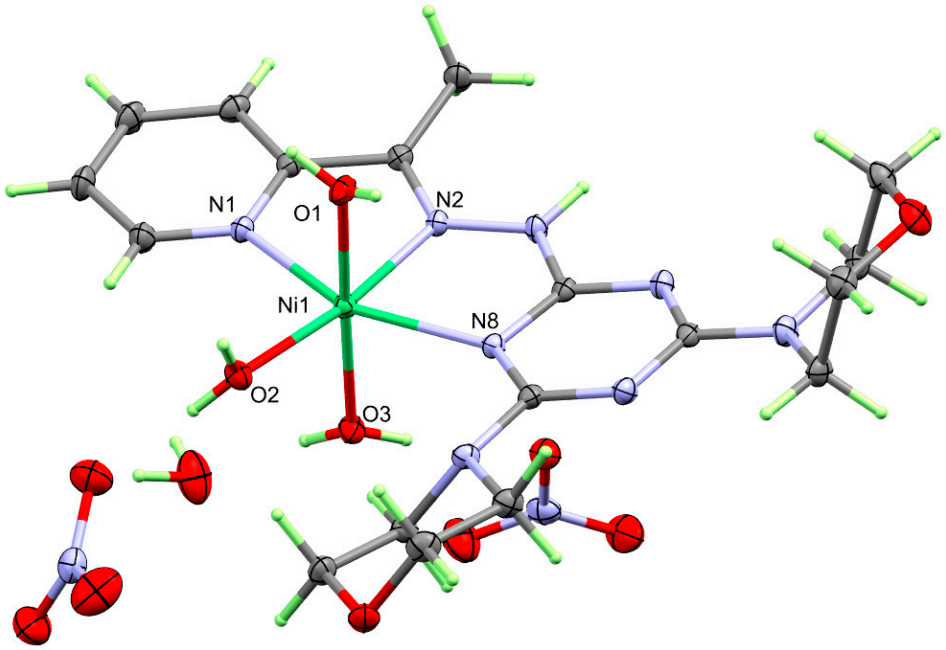

Figure 4. Asymmetric unit of the $[Ni(DMPT)(H_2O)_3](NO_3)_2$. H_2O complex (**2**).

The supramolecular structure of complex **2** is controlled only by a significant number of O . . . H interactions (Table 4), which are considered as another major difference between the two complexes. In this case, there is one crystal water molecule, and hence, the monomeric units are connected differently in the crystal structure compared to **1**. While the hydrazone NH group participated in the hydrogen bond network of **1** by only the N(3)–H(3) . . . O(8) hydrogen bond, there are two significant N–H . . . O hydrogen bonds in complex **2**, which are the N(3)–H(3)...O(6) and N(3)–H(3)...O(7). Additionally, the crystal water molecule is both a hydrogen bond donor and acceptor in this complex via O(3)–H(3A)...O(12), O(12)–H(12C)...O(11) and O(12)–H(12D)...O(9) hydrogen bonds (Figure 5A). In addition, the two morpholine moieties and the nitrate counter anions participated in the hydrogen bonding interactions as hydrogen bond acceptors via their oxygen atoms. A view of the packing scheme is shown in Figure 5B.

Table 3. Bond distances and angles (Åand °) for the coordination environment of $[Ni(DMPT)(H_2O)_3](NO_3)_2.H_2O$ complex.

Bond	**Distance**	**Bond**	**Distance**
Ni(1)–N(2)	2.0079(18)	Ni(1)–O(1)	2.0652(16)
Ni(1)–O(2)	2.0378(17)	Ni(1)–N(1)	2.1031(18)
Ni(1)–O(3)	2.0409(17)	Ni(1)–N(8)	2.1907(18)
Bonds	**Angle**	**Bonds**	**Angle**
N(2)–Ni(1)–O(2)	172.54(7)	O(3)–Ni(1)–N(1)	93.97(7)
N(2)–Ni(1)–O(3)	94.34(7)	O(1)–Ni(1)–N(1)	91.21(7)
O(2)–Ni(1)–O(3)	90.20(8)	N(2)–Ni(1)–N(8)	77.95(7)
N(2)–Ni(1)–O(1)	88.89(7)	O(2)–Ni(1)–N(8)	108.09(7)
O(2)–Ni(1)–O(1)	87.08(7)	O(3)–Ni(1)–N(8)	88.99(7)
O(3)–Ni(1)–O(1)	174.37(7)	O(1)–Ni(1)–N(8)	87.17(7)
N(2)–Ni(1)–N(1)	78.11(7)	N(1)–Ni(1)–N(8)	156.03(7)
O(2)–Ni(1)–N(1)	95.69(7)		

Table 4. The hydrogen bond geometric parameters in $[Ni(DMPT)(H_2O)_3](NO_3)_2.H_2O$.

D–H . . . A	**D–H/Å**	**H . . . A/Å**	**D . . . A/Å**	**D–H . . . A/°**	**Symm. Code**
C(12)–H(12B)...O(7)#1	0.99	2.43	3.122(3)	126.9	#1 x, y + 1, z
N(3)–H(3)...O(6)#2	0.88(3)	2.06(3)	2.930(3)	168(3)	#2 −x + 1, −y + 1, −z + 1
N(3)–H(3)...O(7)#2	0.88(3)	2.60(3)	3.170(3)	123(2)	#2 −x + 1, −y + 1, −z + 1
O(2)–H(2A)...O(9)	0.83(3)	1.96(3)	2.773(3)	168(3)	
O(1)–H(1A)...O(4)#3	0.81(3)	1.91(4)	2.691(2)	161(3)	#3 −x + 1, −y + 2, −z + 1
O(1)–H(1B)...O(5)#4	0.86(4)	1.97(4)	2.798(2)	161(3)	#4 x − 1, y, z
O(2)–H(2B)...O(10)#5	0.82(3)	1.96(3)	2.775(3)	175(3)	#5 −x + 1, −y + 1, −z + 2
O(3)–H(3A)...O(12)	0.84(3)	1.85(4)	2.686(3)	170(3)	
O(3)–H(3B)...O(6)	0.82(4)	1.95(4)	2.757(3)	171(4)	
O(3)–H(3B)...O(8)	0.82(4)	2.57(4)	3.184(3)	134(3)	
O(12)–H(12C)...O(11)#6	0.80(4)	2.10(4)	2.885(4)	165(4)	#6 −x + 1, −y, −z + 2
O(12)–H(12D)...O(9)	1.01(6)	1.91(6)	2.841(3)	152(5)	

In the studied complexes, we noted the presence of another common intermolecular interaction between the nitrate anion and the π-system of the organic ligand (DMPT). It is clearly seen from Figure 6 that the presence of short C6 . . . O9 (3.108 Å) and C8 . . . O6 (3.208 Å) contacts revealed this observation very well.

2.3. Hirshfeld Analysis

The results of the X-ray crystal structure analysis were accurately mirrored by the Hirshfeld surface analysis, which also provided a novel visual way to understand intermolecular interactions via the colors of various regions [46,47]. The Hirshfeld (HF) surfaces and the 2D fingerprint (FP) plots of complexes **1** and **2** were analyzed. As shown from X-ray studies, the asymmetric unit in complex **1** consists of one $[Ni(DMPT)(H_2O)_3]^{2+}$ cationic complex unit as the inner sphere and two nitrate anions in addition to three crystallized water molecules in the outer sphere. On the other hand, there is only one water molecule present in an asymmetric unit of complex **2**. Hence, the Hirshfeld surfaces around each entity in both complexes have been computed (Figure 7). Using fingerprint plot, it is possible to decompose all intermolecular interactions and the percentage of all these contacts could be easily obtained. Subsequently, their corresponding intermolecular interactions were quantified separately in Figure 8.

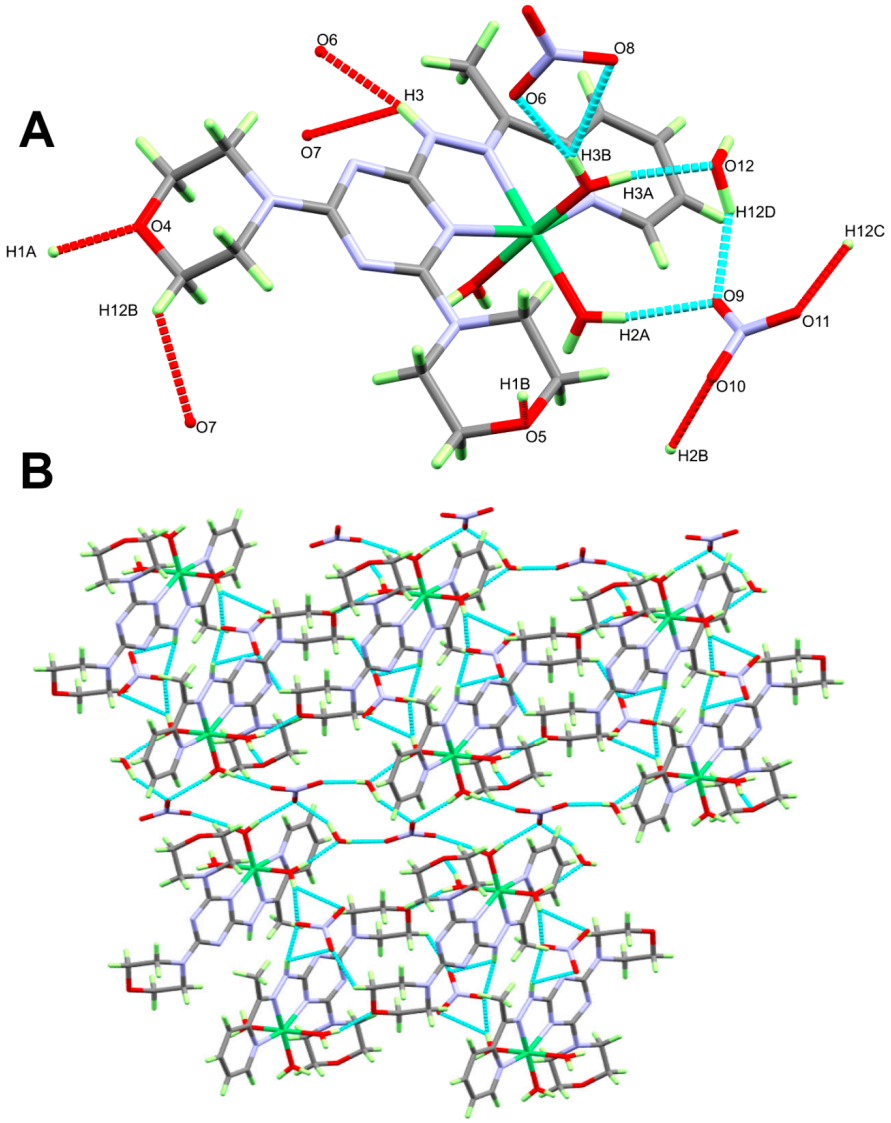

Figure 5. All of the important hydrogen bond contacts (**A**) and 3D H-bonding network (**B**) in $[Ni(DMPT)(H_2O)_3](NO_3)_2.H_2O$ complex.

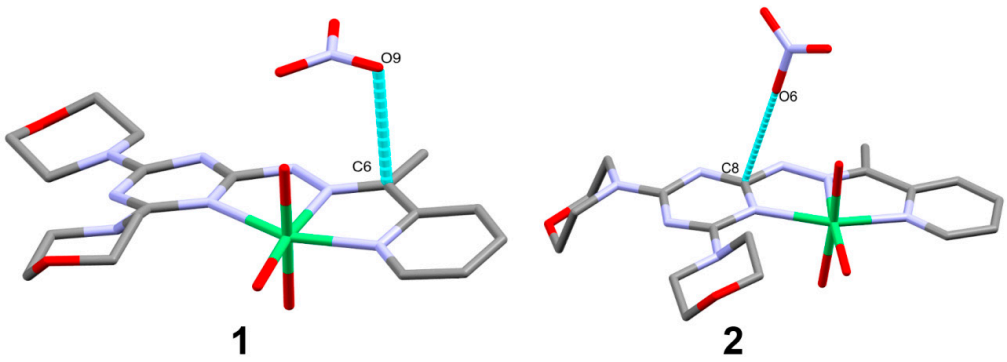

Figure 6. The anion–π interactions in complexes **1** and **2**.

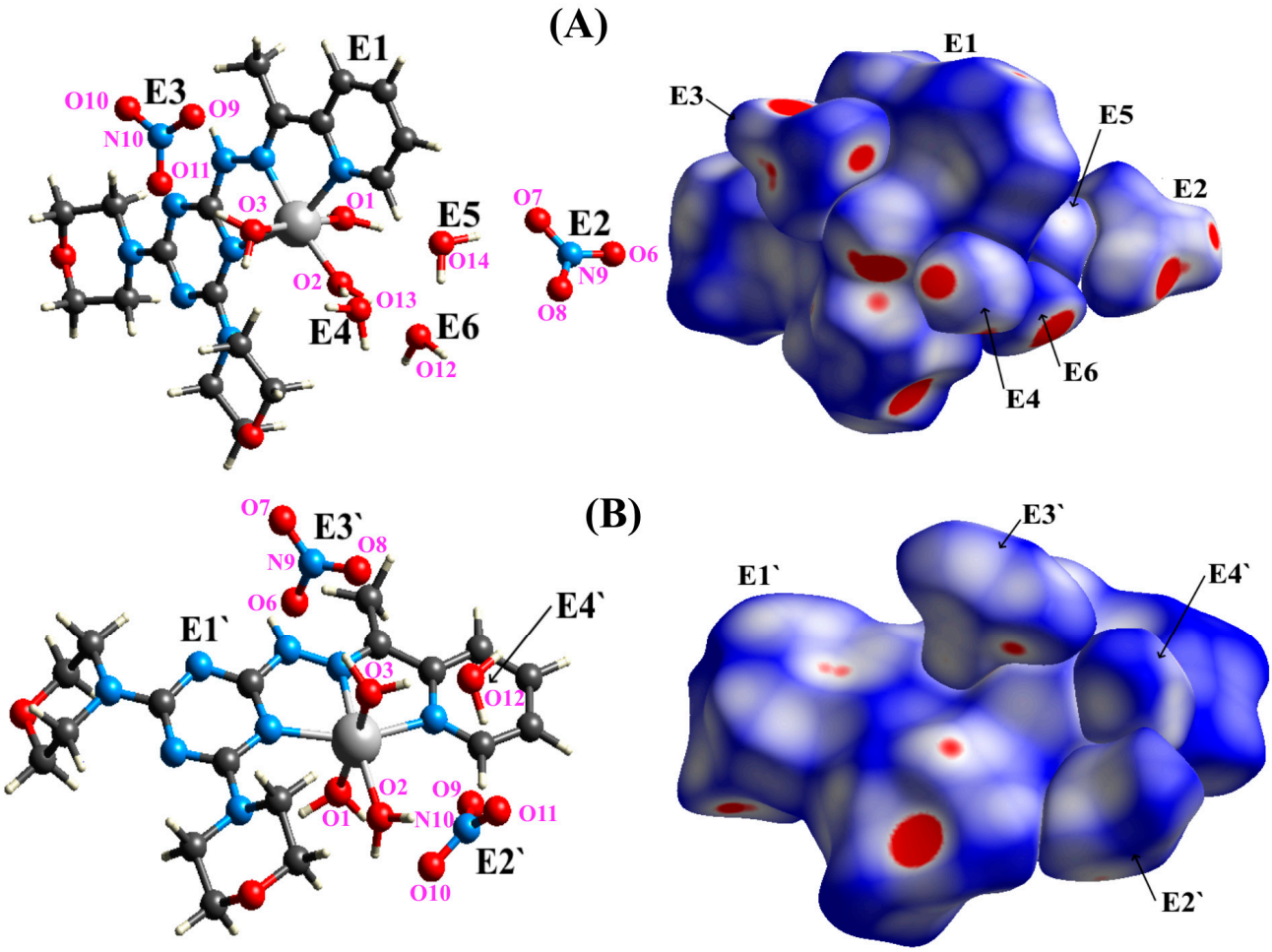

Figure 7. The d_{norm} maps of the HF surface for all entities in complexes **1** (**A**) and **2** (**B**).

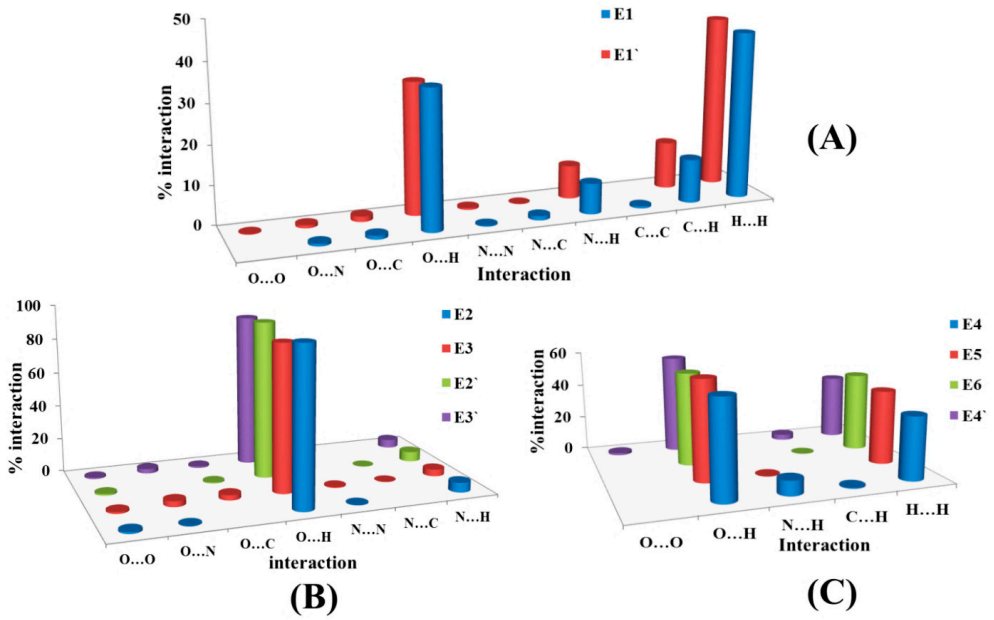

Figure 8. Distribution of the intermolecular interactions for the $[Ni(DMPT)(H_2O)_3]^{2+}$ cation (**A**), outer-sphere nitrate anions (**B**) and hydrated water molecules (**C**) in both complexes.

According to the aforementioned data, both complexes (**1** and **2**) are very close in their intermolecular interactions. It is clear that the interactions involving hydrogen atoms are the most dominant, mainly the hydrogenic H . . . H and the polar O . . . H interactions in all entities, except nitrate anions, in which the O . . . H interaction is the only most prevalent one (Figure 8). This suggests that strong O . . . H interactions is the driving force in the formation of the crystal packing in both complexes, and this is attributed to the presence of the nitrate anions and water molecules.

For the $[Ni(DMPT)(H_2O)_3]^{2+}$ cation (E1 and E1′ in complexes **1** and **2**, respectively), the most significant contact is the O . . . H interaction, which contributed by 35.1 and 33.5% in E1 and E1′, respectively. Additionally, the H . . . H, N . . . H and C . . . H contacts contributed 42.3, 7.8 and 11.1% in E1, respectively. The corresponding values in E1′ are 43.3, 8.5 and 11.9%, respectively. These short interactions appeared as sharp spikes in the FP plots (Figure 9), indicating strong interactions between the $[Ni(DMPT)(H_2O)_3]^{2+}$ and the neighboring units (Figure 10 and Table 5). In the entity E1 of complex **1**, the shortest O . . . H interactions are O13 . . . H2B (1.710Å), O12 . . . H2A (1.749 Å) and O14 . . . H1A (1.656 Å). On the other hand, the O12 . . . H3A (1.713 Å) and O4 . . . H1A (1.749 Å) in the E1′ entity of complex **2** are the most significant O . . . H contact. A summary of the significant short interactions around the $[Ni(DMPT)(H_2O)_3]^{2+}$ in both complexes is shown in Table 5.

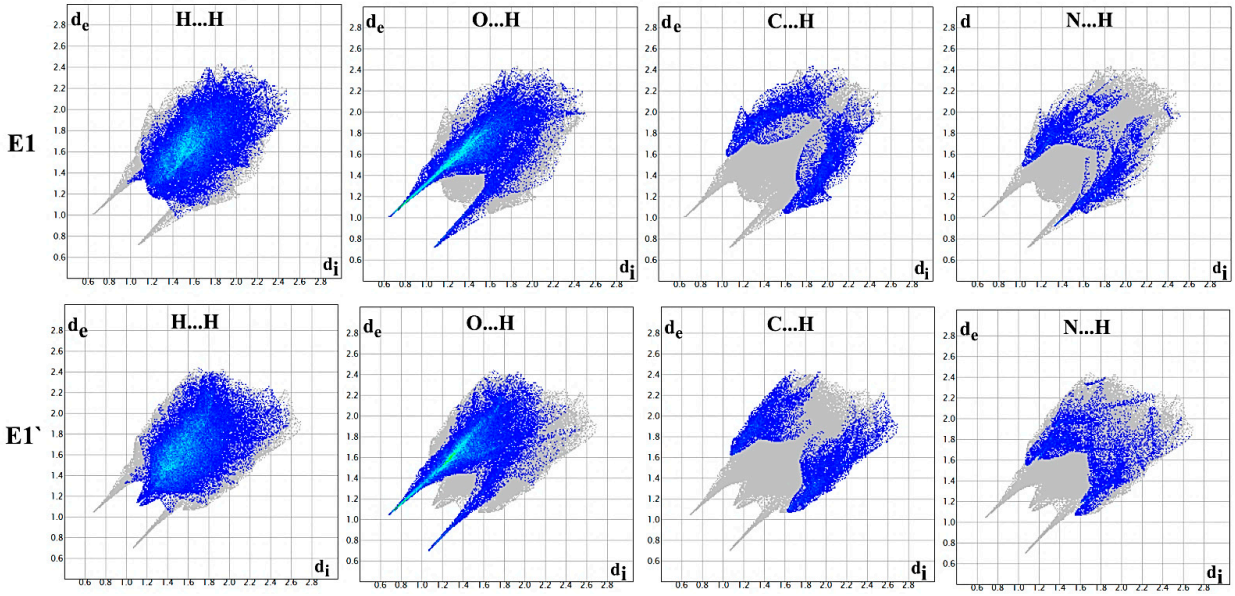

Figure 9. Decomposed FP plots of the major contacts around the $[Ni(DMPT)(H_2O)_3]^{2+}$ cation units E1 and E1′ in complexes **1** and **2**, respectively.

For the outer-sphere nitrate anions (E2 and E3 in **1**, while E2′and E3′ in **2**), the O...H contact is the most dominant, which contributed 92.5% (E2), 86.6% (E3), 92.3% (E2′) and 89.6% (E3′) of the total HF surface area (Figure 11). The shortest contacts which appeared in the d_{norm} maps as red spots are O7 . . . H14B (1.829Å) and O11 . . . H3B (1.779 Å) in complex **1**, while O10 . . . H2B (1.794 Å) and O6 . . . H3B (1.784 Å) in complex **2** (Table 5).

For the water of crystallization (E4:E6 in **1** and E4′ in **2**), the O . . . H and H . . . H interactions represent almost all the 2D fingerprint area (Figure S2, Supplementary Data). The decomposed d_{norm} maps exemplify relatively short O . . . H and H . . . H interactions that appear as dark red spots (Figure 12). The shortest O . . . H contacts in **1** are O13 . . . H2B (1.710 Å), O14 . . . H1A (1.656 Å) and O12 . . . H2A (1.749 Å), while O12 . . . H3A (1.713 Å) in **2**. For the H . . . H interaction, the shortest contacts are H13D . . . H2B (2.152Å), H14A . . . H1A (2.118 Å) and H12D . . . H3A (2.151Å), as shown in Table 5.

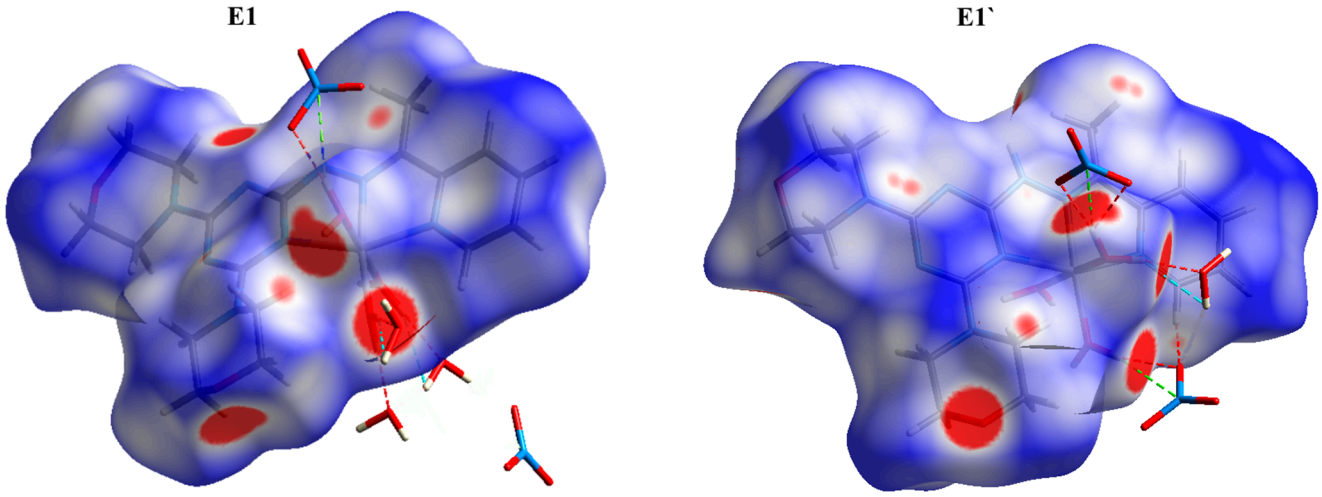

Figure 10. The shortest intermolecular interactions around E1 and E1′ entities. The red, turquoise and green dotted lines represent the O . . . H, H . . . H and N . . . H contacts, respectively.

Table 5. Distances (**Å**) of the significant short interactions in both complexes.

Complex 1		Complex 2	
Contact	**Distance**	**Contact**	**Distance**
O11 . . . H3B	1.779	O8 . . . H3B	2.453
O13 . . . H2B	1.710	O6 . . . H3B	1.784
O12 . . . H2A	1.749	O9 . . . H2A	1.806
O14 . . . H1A	1.656	O9 . . . H1	2.533
O5 . . . H12D	1.829	O12 . . . H3A	1.713
O6 . . . H3A	1.854	O5 . . . H1B	1.855
O7 . . . H3A	2.439	O7 . . . H12B	2.371
O4 . . . H1B	1.793	O4 . . . H1A	1.749
O9 . . . H11B	2.300	O5 . . . H1B	1.855
O8 . . . H3	1.950	O10 . . . H2B	1.794
O6 . . . H3	2.528	O6 . . . H7B	2.573
O11 . . . H3C	2.508	O8 . . . H4	2.449
O7 . . . H4	2.405	O6 . . . H7A	2.458
O10 . . . H16B	2.561	O6 . . . H3	1.937
O11 . . . H16B	2.530	O7 . . . H3	2.535
O7 . . . H14B	1.829	O9 . . . H12D	1.932
O8 . . . H14B	2.585	O11 . . . H12C	1.928
O6 . . . H13C	2.333	O6 . . . C8	3.208
O9 . . . H12C	2.361	N10 . . . H2A	2.555
O10 . . . H12C	1.897	N9 . . . H3B	2.465
O10 . . . H13D	1.903	N5 . . . H7C	2.588
O11 . . . H13D	2.523	C5 . . . H18A	2.660
O12 . . . H14A	1.795	C16 . . . H1B	2.704
N5 . . . H13C	2.251	C12 . . . H1A	2.593
N10 . . . H16B	2.519	C9 . . . H12A	2.697
N10 . . . H3B	2.555	C9 . . . H7C	2.708
N9 . . . H14B	2.536	H12D . . . H3A	2.151
C9 . . . H10A	2.633		
C4 . . . H18A	2.706		
C17 . . . H12D	2.430		
H1A . . . H14A	2.118		
H2B . . . H13D	2.152		

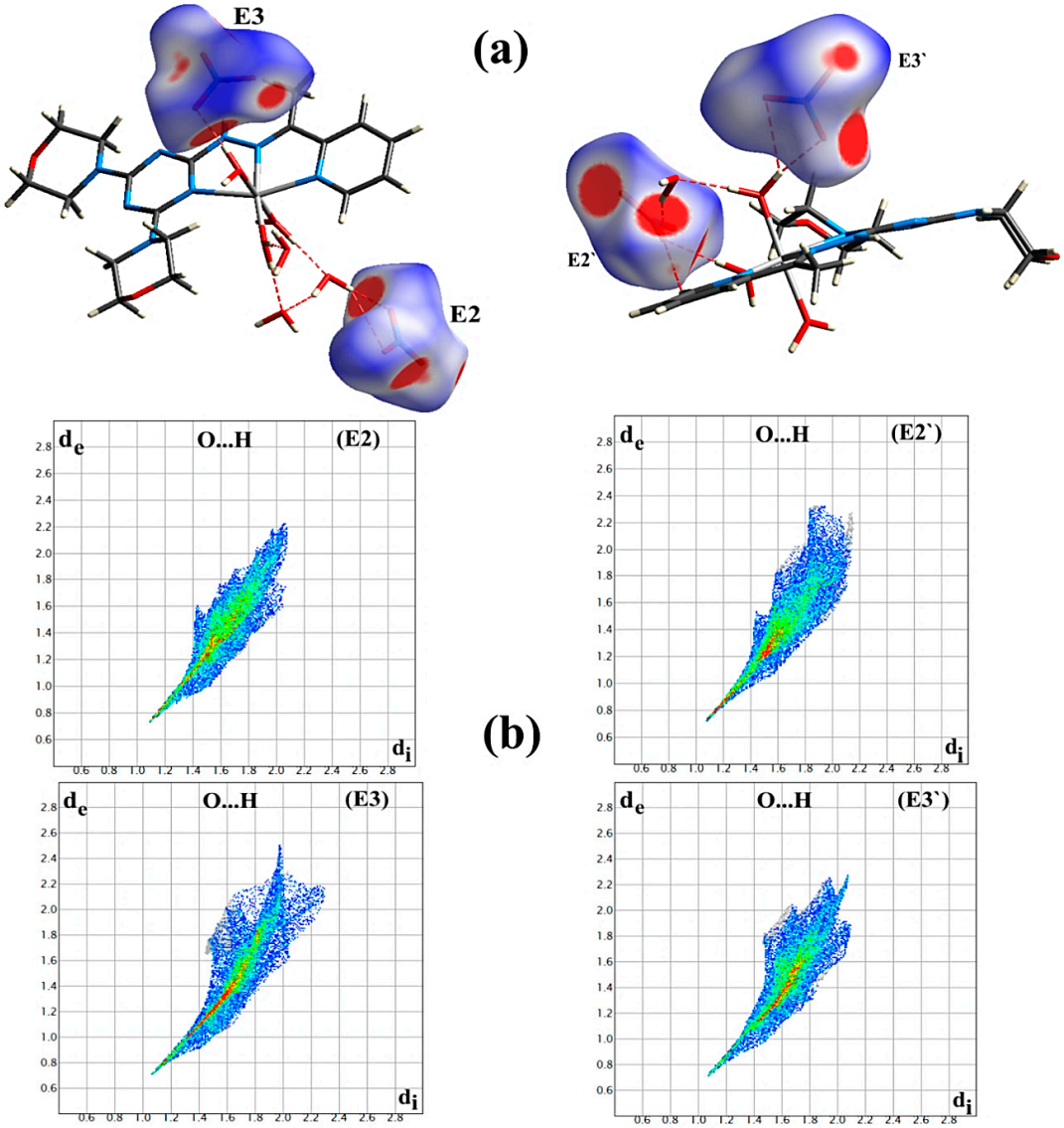

Figure 11. The d_{norm} maps of the nitrate anions showing the O . . . H interactions (**a**) and their corresponding FP plots (**b**).

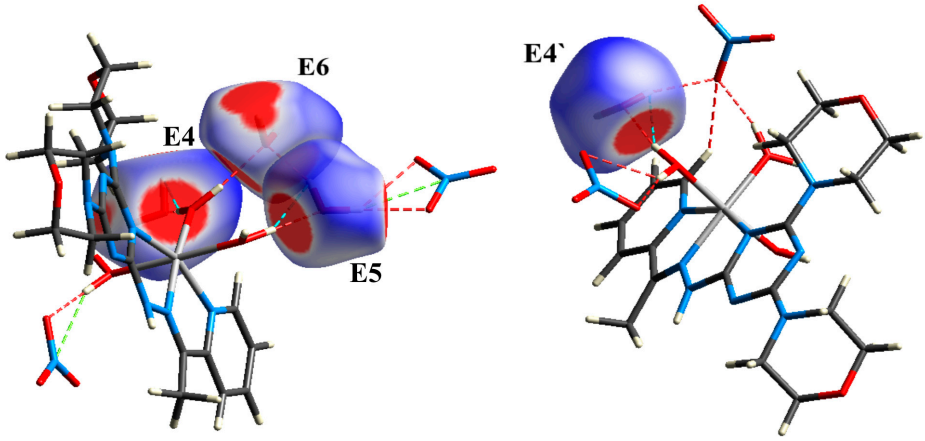

Figure 12. The d_{norm} maps showing the short contacts between crystal water molecules and other entities. The red, turquoise and green dotted lines represent the O . . . H, H . . . H and N . . . H contacts, respectively.

2.4. Antimicrobial Assay

The antimicrobial activity of the free ligand and complex **1** were determined against selected Gram-positive, Gram-negative bacterial strains and two fungal species. The results of the inhibition zone diameters were collected in Table 6. The results indicated that both the ligand and its Ni(II) complex are inactive toward both fungal species: *A. fumigatus* and *C. albicans*. On the other hand, the Ni(II) complex was found active against the Gram-positive bacterial species *B. subtilis,* but not active against *S.aureus*. The inhibition zone diameter of the Ni(II) complex is 12 mm and the minimum inhibitory concentration is 1250 µg/mL. Additionally, the Ni(II) complex is active against the Gram-negative bacterial species *E. coli,* but is found inactive against *P. vulgaris.* The inhibition zone diameter of the Ni(II) complex is 11 mm and the minimum inhibitory concentration is 1250 µg/mL. Interestingly, the free ligand was found inactive against both Gram-positive and Gram-negative bacteria species. The higher antibacterial activity of the Ni(II) complex against *B. subtilis* and *E. coli* compared to the free Schiff base ligand (DMPT) might be attributed to the ability of the metal chelates to inhibit the respiration mechanism of the microbial organisms, which make them unable to manufacture their own proteins, preventing the organism from growing further [48]. On the other hand, the studied Ni(II) complex has a lower antimicrobial activity than the *gentamycin* as a positive control. It is worth to note that the Cu(II) and Mn(II) complexes of DMPT ligand [45] are better antimicrobial agents and have broader antibacterial spectra than the corresponding Ni(II) complex.

Table 6. Antibacterial and antifungal activities of DMPT and its Ni(II) complex in terms of inhibition zone diameters (mm) and MIC (µg/mL) [a].

Microorganism	DMPT	1	Control
A. fumigatus	NA [b] (ND) [c]	NA [b] (ND) [c]	17(156) [d]
C. albicans	NA [b] (ND) [c]	NA [b] (ND) [c]	20(312) [d]
S. aureus	NA [b] (ND) [c]	NA [b] (ND) [c]	24(9.7) [e]
B. subtilis	NA [b] (ND) [c]	12 (1250) [c]	26(4.8) [e]
E. coli	NA [b] (ND) [c]	11 (1250) [c]	30(4.8) [e]
P. vulgaris	NA [b] (ND) [c]	NA [b] (1250) [c]	25(4.8) [e]

[a] Values outside and inside parentheses for inhibition zone diameter and MIC, respectively. [b] NA: No activity; [c] ND: not determined; [d] ketoconazole and [e] *gentamycin.*

3. Materials and Methods

3.1. Physical Measurements

All the chemicals were bought from Sigma-Aldrich and used without additional purifications. CHN analyses were carried out using a PerkinElmer 2400 Elemental Analyzer. The amount of Ni was determined with the aid of a Shimadzu atomic absorption spectrophotometer (AA-7000 series, Shimadzu, Ltd., Tokyo, Japan). FTIR spectra were recorded at the Central Lab, Faculty of Science, Alexandria University, using a Bruker Tensor 37 FTIR spectrophotometer (Bruker Company, Berlin, Germany) in KBr pellets at 4000–400 cm^{-1}.

3.2. Preparation of DMPT

3.2.1. Synthesis of Ligand (DMPT) [45]

s-Triazine hydrazine derivative (2 mmol, 563 mg) mixed with 2-acetylpyridine (2 mmol, 242 mg) in ethanol (20 mL in the presence of a drop of acetic acid and then refluxed overnight; the reaction was monitored by (TLC 2% MeOH/$CHCl_3$ then 50:50 EtOAc/n-hexane). After evaporation 1/3 of the solvent the desired product was precipitated as white powered materials and then filtered and washed with a small quantity of ethanol to afford the requisite ligand (DMPT).

Ligand (DMPT): m.p: 230 °C; ^{1}H NMR (400 MHz, $CDCl_3$) δ 8.54 (d, *J* = 4.6 Hz, 1H), 8.20 (d, *J* = 8.1 Hz, 1H), 8.08 (s, 1H), 7.67 (t, *J* = 8.0 Hz, 1H), 7.20 (dd, *J* = 7.3, 4.9 Hz, 1H), 3.81 (q, *J* = 8.2, 6.4 Hz, 8H), 3.72 (t, *J* = 4.8 Hz, 8H), 2.40 (s, 3H) ppm. ^{13}C NMR (101 MHz, $CDCl_3$)

δ 165.36, 164.61, 155.63, 148.48, 147.51, 139.00, 136.27, 123.68, 119.89, 66.95, 43.75 ppm. IR (KBr, cm^{-1}): 3442 ν (N–H), 2962, 2895, 2855 ν(C–H), 1606, 1584 ν(C=N), 1523, 1492 ν(C=C), 1256 ν(C–N).

3.2.2. Synthesis of Complexes $[Ni(DMPT)(H_2O)_3](NO_3)_2.3H_2O$ (1) and $[Ni(DMPT)(H_2O)_3](NO_3)_2.H_2O$ (2)

Equimolar amounts of 15 mL ethanolic solution of $Ni(NO_3)_2.6H_2O$ (29.1 mg, 0.1 mmol) and 15 mL ethanolic solution of organic ligand DMPT (38.4 mg, 0.1 mmol) were added into one pot. The resulting clear green solution was allowed to evaporate slowly and crystallize at room temperature. After one week, green crystals of complex **1** were collected from the walls of the glass beaker, whereas turquoise crystals of **2** were collected from the bottom of the beaker. The crystals were left for drying and used for single-crystal X-ray diffraction measurement.

Complex **1**, Anal. Calc. $C_{18}H_{36}N_{10}NiO_{14}$: C, 32.02; H, 5.37; N, 20.74; Ni, 8.69%. Found: C, 31.61; H, 5.26; N, 20.63; Ni, 8.47%. IR (KBr, cm^{-1}): 3382 ν(O–H) $_{water}$, 3246 ν (N–H), 2977, 2930, 2860 ν(C–H), 1593, 1572 ν(C=N), 1509 ν(C=C), 1385 ν(N–O),1260 ν(C–N), 785 ρ_r (H_2O), 641ρ_w (H_2O).

Complex **2**, Anal. Calc. $C_{18}H_{32}N_{10}NiO_{12}$: C, 33.82; H, 5.05; N, 21.91; Ni, 9.18%. Found: C, 33.63; H, 4.98; N, 21.75; Ni, 9.09%. IR (KBr, cm^{-1}): 3327 ν(O–H)$_{water}$, 3247 ν (N–H), 2959, 2929, 2864 ν(C–H), 1607, 1575 ν(C=N), 1509 ν(C=C), 1385 ν(N–O),1259 ν(C–N), 809 ρ_r (H_2O), 634 ρ_w (H_2O).

3.3. X-ray Crystallography

The experimental measurements [49–54] for the complexes **1** and **2** are provided in the Supplementary Materials. Crystal data of complexes **1** and **2** are presented in Table S1.

3.4. Hirshfeld Analysis

The Crystal Explorer Ver. 3.1 program [55] was used to perform this analysis.

3.5. Antimicrobial Assay

Using the procedure mentioned in Method S1 (Supplementary Data), the antibacterial activities [56] of DMPT and complexes **1** and **2** toward several microbes were determined.

4. Conclusions

Using analytical and spectroscopic techniques, the structures of the recently synthesized Ni(II) complexes were determined as $[Ni(DMPT)(H_2O)_3](NO_3)_2.3H_2O$ (1) and $[Ni(DMPT)(H_2O)_3](NO_3)_2.H_2O$ (2). The structures of complexes **1** and **2** were very similar regarding the coordination sphere and counter anions, but differ only in the number of the crystal water molecules. The inner spheres of both complexes comprised a hexa-coordinated Ni(II) ion with one DMPT and three water molecules with a distorted octahedral coordination environment, while the outer sphere composed of two nitrate counter ions in addition to three crystal water molecules in complex **1** compared to only one crystallized water molecule in complex **2**. The DMPT ligand acts as a neutral tridentate *NNN*-chelate via three Ni–N coordination interactions. The supramolecular structures of **1** and **2** were described on the basis of a Hirshfeld analysis along side an X-ray single-crystal diffraction. The Hirshfeld surfaces around each entity in both complexes have been computed. The hydrogenic H . . . H and the polar O . . . H interactions are the most dominant. Additionally, the presence of short C6...O9 (3.108 Å) and C8...O6 (3.208 Å) contacts in complexes **1** and **2**, respectively, revealed the presence of anion–π stacking interactions. The organic ligands have no antimicrobial activity against the studied microbes at the applied concentration. In contrast, the Ni(II) complex **1** showed antimicrobial activity against *Bacillus subtilis* and *Escherichia coli*.

Supplementary Materials: The following supporting information can be downloaded at: https://www.mdpi.com/article/10.3390/inorganics11050222/s1, X-Ray structure determinations; Table S1. Crystal Data; Evaluation of antimicrobial activity [56]; Figure S1. FTIR spectra of complexes **1** and **2** compared to the free ligand DMPT; Figure S2. The 2D fingerprint plots of the major contacts around the water moieties (E4, E5, E6 in complex **1** and E4′ in complex **2**).

Author Contributions: Conceptualization, M.A.M.A.-Y. and S.M.S.; formal analysis, E.M.F., M.M.S. and M.H.; investigation, E.M.F.; methodology, E.M.F. and A.B.; software, M.H. and S.M.S.; supervision, M.A.M.A.-Y., A.B. and S.M.S.; validation, A.E.-F. and A.B.; Funding acquisition: A.B.; visualization, A.E.-F.; writing—original draft, S.M.S.; writing—review and editing, M.A.M.A.-Y., A.E.-F. and A.B. All authors have read and agreed to the published version of the manuscript.

Funding: The authors would like to extend their sincere appreciation to the Researchers Supporting Project (RSP2023R64), King Saud University, Riyadh, Saudi Arabia.

Institutional Review Board Statement: Not applicable.

Informed Consent Statement: Not applicable.

Data Availability Statement: Not applicable.

Conflicts of Interest: The authors declare no conflict of interest.

References

1. Wu, P.; Ma, D.-L.; Leung, C.-H.; Yan, S.-C.; Zhu, N.; Abagyan, R.; Che, C.-M. Stabilization of G-Quadruplex DNA with Platinum(II) Schiff Base Complexes: Luminescent Probe and Down-Regulation of c-*myc*Oncogene Expression. *Chem. A Eur. J.* **2009**, *15*, 13008–13021. [CrossRef] [PubMed]
2. Kumar, S.; Dhar, D.N.; Saxena, P.N. Applications of metal complexes of Schiff bases-A review. *J. Sci. Ind. Res.* **2009**, *68*, 181–187.
3. Grivani, G.; Ghavami, A.; Kučeráková, M.; Dušek, M.; Khalaji, A.D. Synthesis, characterization, crystal structure determination, thermal study and catalytic activity of a new oxidovanadium Schiff base complex. *J. Mol. Struct.* **2014**, *1076*, 326–332. [CrossRef]
4. Liu, X.; Manzur, C.; Novoa, N.; Celedón, S.; Carrillo, D.; Hamon, J.-R. Multidentate unsymmetrically-substituted Schiff bases and their metal complexes: Synthesis, functional materials properties, and applications to catalysis. *Coord. Chem. Rev.* **2018**, *357*, 144–172. [CrossRef]
5. Ghaffari, A.; Behzad, M.; Pooyan, M.; Rudbari, H.A.; Bruno, G. Crystal structures and catalytic performance of three new methoxy substituted salen type nickel (II) Schiff base complexes derived from meso-1, 2-diphenyl-1, 2-ethylenediamine. *J. Mol. Struct.* **2014**, *1063*, 1–7. [CrossRef]
6. Li, L.-J.; Yang, L.-K.; Chen, Z.-K.; Huang, Y.-Y.; Fu, B.; Du, J.-L. Synthesis and characterization of multifunctional Schiff base and Cu(II) complex: Degradation of organic dyes and an optical property investigation. *Inorg. Chem. Commun.* **2014**, *50*, 62–64. [CrossRef]
7. Fan, H.-T.; Liu, J.-X.; Sui, D.-P.; Yao, H.; Yan, F.; Sun, T. Use of polymer-bound Schiff base as a new liquid binding agent of diffusive gradients in thin-films for the measurement of labile Cu2+, Cd2+ and Pb2+. *J. Hazard. Mater.* **2013**, *260*, 762–769. [CrossRef]
8. Masuya, A.; Igarashi, C.; Kanesato, M.; Hoshino, H.; Iki, N. One-pot synthesis and structural characterization of a Tb(III) coordination polymer based on a tripodal Schiff base ligand adopting an exo-bridging coordination mode. *Polyhedron* **2015**, *85*, 76–82. [CrossRef]
9. Neelakantan, M.; Esakkiammal, M.; Mariappan, S.; Dharmaraja, J.; Jeyakumar, T. Synthesis, Characterization and Biocidal Activities of Some Schiff Base Metal Complexes. *Indian J. Pharm. Sci.* **2010**, *72*, 216. [CrossRef]
10. Patil, A.R.; Donde, K.J.; Raut, S.S.; Patil, V.R.; Lokhande, R.S. Synthesis, characterization and biological activity of mixed ligand Co(II) complexes of schiff base 2-amino-4-nitrophenol-n-salicylidene with some amino acids. *J. Chem. Pharm. Res.* **2012**, *4*, 1413–1425.
11. Salehi, M.; Rahimifar, F.; Kubicki, M.; Asadi, A. Structural, spectroscopic, electrochemical and antibacterial studies of some new nickel (II) Schiff base complexes. *Inorg. Chim. Acta* **2016**, *443*, 28–35. [CrossRef]
12. Chandra, S. Ruchi Synthesis, spectroscopic characterization, molecular modeling and antimicrobial activities of Mn(II), Co(II), Ni(II), Cu(II) complexes containing the tetradentate aza Schiff base ligand. *Spectrochim. Acta Part A Mol. Biomol. Spectrosc.* **2013**, *103*, 338–348. [CrossRef]
13. Bharti, S.; Choudhary, M.; Mohan, B.; Rawat, S.; Sharma, S.; Ahmad, K. Syntheses, characterization, superoxide dismutase, antimicrobial, crystal structure and molecular studies of copper (II) and nickel (II) complexes with 2-((E)-(2, 4-dibromophenylimino) methyl)-4-bromophenol as Schiff base ligand. *J. Mol. Struct.* **2017**, *1149*, 846–861. [CrossRef]
14. Layek, S.; Agrahari, B.; Tarafdar, A.; Kumari, C.; Ganguly, R.; Pathak, D.D. Synthesis, spectroscopic and single crystal X-ray studies on three new mononuclear Ni(II) pincer type complexes: DFT calculations and their antimicrobial activities. *J. Mol. Struct.* **2017**, *1141*, 428–435. [CrossRef]
15. Chandra, S.; Agrawal, S. Spectroscopic characterization of Lanthanoid derived from a hexadentate macrocyclic ligand: Study on antifungal capacity of complexes. *Spectrochim. Acta Part A Mol. Biomol. Spectrosc.* **2014**, *124*, 564–570. [CrossRef] [PubMed]

16. Kumar, S.; Devi, J.; Dubey, A.; Kumar, D.; Jindal, D.K.; Asija, S.; Sharma, A. Co(II), Ni(II), Cu(II) and Zn(II) complexes of Schiff base ligands: Synthesis, characterization, DFT, in vitro antimicrobial activity and molecular docking studies. *Res. Chem. Intermed.* **2023**, *49*, 939–965. [CrossRef]
17. Tyagi, M.; Chandra, S.; Akhtar, J.; Chand, D. Modern spectroscopic technique in the characterization of biosensitive macrocyclic Schiff base ligand and its complexes: Inhibitory activity against plantpathogenic fungi. *Spectrochim. Acta Part A Mol. Biomol. Spectrosc.* **2014**, *118*, 1056–1061. [CrossRef]
18. Sathiyaraj, S.; Sampath, K.; Butcher, R.J.; Pallepogu, R.; Jayabalakrishnan, C. Designing, structural elucidation, comparison of DNA binding, cleavage, radical scavenging activity and anticancer activity of copper (I) complex with 5-dimethyl-2-phenyl-4-[(pyridin-2-ylmethylene)-amino]-1, 2-dihydro-pyrazol-3-one Schiff base ligand. *Europ. J. Med. Chem.* **2013**, *64*, 81–89. [CrossRef]
19. Khan, S.; Ibrahim, M.M.; Alhumaydhi, F.A.; Alqahtani, A.; Alshamrani, M.; Alruwaili, A.S.; Hassanian, A.A.; Khan, S. Recent advances and therapeutic journey of Schiff base complexes with selected metals (Pt, Pd, Ag, Au) as potent anticancer agents: A review. *Anti-Cancer Agents Med. Chem.* **2022**, *22*, 3086–3096. [CrossRef]
20. Odularu, A.T. Manganese Schiff base complexes, crystallographic studies, anticancer activities, and molecular docking. *J. Chem.* **2022**, *2022*, 7062912. [CrossRef]
21. Chen, G.J.; Qiao, X.; Qiao, P.Q.; Xu, G.J.; Xu, J.Y.; Tian, J.L.; Gu, W.; Liu, X.; Yan, S.P. Synthesis, DNA binding, photo-induced DNA cleavage, cytotoxicity and apoptosis studies of copper (II) complexes. *J. Inorg. Biochem.* **2011**, *105*, 119–126. [CrossRef] [PubMed]
22. Elshafie, H.S.; Sadeek, S.A.; Camele, I.; Mohamed, A.A. Biochemical Characterization of New Gemifloxacin Schiff Base (GMFX-o-phdn) Metal Complexes and Evaluation of Their Antimicrobial Activity against Some Phyto- or Human Pathogens. *Int. J. Mol. Sci.* **2022**, *23*, 2110. [CrossRef] [PubMed]
23. Angelusiu, M.V.; Barbuceanu, S.-F.; Draghici, C.; Almajan, G.L. New Cu(II), Co(II), Ni(II) complexes with aroyl-hydrazone based ligand. Synthesis, spectroscopic characterization and in vitro antibacterial evaluation. *Eur. J. Med. Chem.* **2010**, *45*, 2055–2062. [CrossRef] [PubMed]
24. Wang, Q.; Yang, Z.-Y.; Qi, G.-F.; Qin, D.-D. Crystal structures, DNA-binding studies and antioxidant activities of the Ln(III) complexes with 7-methoxychromone-3-carbaldehyde-isonicotinoyl hydrazone. *Biometals* **2009**, *22*, 927–940. [CrossRef]
25. Aslan, H.G.; Özcan, S.; Karacan, N. Synthesis, characterization and antimicrobial activity of salicylaldehyde benzenesulfonylhydrazone (Hsalbsmh) and its nickel (II), palladium (II), platinum (II), copper (II), cobalt (II) complexes. *Inorg. Chem. Commun.* **2011**, *14*, 1550–1553. [CrossRef]
26. Naskar, S.; Naskar, S.; Butcher, R.J.; Chattopadhyay, S.K. Synthesis, X-ray crystal structures and spectroscopic properties of two Ni(II) complexes of pyridoxal Schiff's bases with diamines: Importance of steric factor in stabilization of water helices in the lattices of metal complex. *Inorg. Chim. Acta* **2010**, *363*, 404–411. [CrossRef]
27. Xu, Z.H.; Zhang, X.W.; Zhang, W.Q.; Gao, Y.H.; Zeng, Z.Z. Synthesis, characterization, DNA interaction and antibacterial activities of two tetranuclear cobalt (II) and nickel (II) complexes with salicylaldehyde 2-phenylquinoline-4-carboylhydrazone. *Inorg. Chem. Commun.* **2011**, *14*, 1569–1573. [CrossRef]
28. Kratz, F.; Beyer, U.; Roth, T.; Tarasova, N.; Collery, P.; Lechenault, F.; Cazabat, A.; Schumacher, P.; Unger, C.; Falken, U. Transferrin Conjugates of Doxorubicin: Synthesis, Characterization, Cellular Uptake, and in Vitro Efficacy. *J. Pharm. Sci.* **1998**, *87*, 338–346. [CrossRef]
29. Sobha, S.; Mahalakshmi, R.; Raman, N. Studies on DNA binding behaviour of biologically active transition metal complexes of new tetradentate N2O2 donor Schiff bases: Inhibitory activity against bacteria. *Spectrochim. Acta Part A Mol. Biomol. Spectrosc.* **2012**, *92*, 175–183. [CrossRef]
30. Hazari, N.; Melvin, P.R.; Beromi, M.M. Well-defined nickel and palladium precatalysts for cross-coupling. *Nat. Rev. Chem.* **2017**, *1*, 0025. [CrossRef]
31. Kar, P.; Yoshida, M.; Shigeta, Y.; Usui, A.; Kobayashi, A.; Minamidate, T.; Matsunaga, N.; Kato, M. Methanol-Triggered Vapochromism Coupled with Solid-State Spin Switching in a Nickel(II)-Quinonoid Complex. *Angew. Chem.* **2017**, *129*, 2385–2389. [CrossRef]
32. Emam, S.M.; AbouEl-Enein, S.A.; Emara, E.M. Spectroscopic studies and thermal decomposition for (bis-((E)-2-(4-ethylphenylimino)-1,2-diphenylethanone) Schiff base and its Co(II), Ni(II), Cu(II), Zn(II) and Cd(II) complexes prepared by direct and template reactions. *J. Therm. Anal. Calorim.* **2017**, *127*, 1611–1630. [CrossRef]
33. Güveli, Ş.; Bal-Demirci, T.; Ülküseven, B.; Özdemir, N. Supramolecular nickel complex based on thiosemicarba-zone. Synthesis, transfer hydrogenation and unexpected thermal behavior. *Polyhedron* **2016**, *110*, 188–196. [CrossRef]
34. Craig, G.A.; Sarkar, A.; Woodall, C.H.; Hay, M.A.; Marriott, K.E.R.; Kamenev, K.V.; Moggach, S.A.; Brechin, E.K.; Parsons, S.; Rajaraman, G.; et al. Probing the origin of the giant magnetic anisotropy in trigonal bipyramidal Ni(ii) under high pressure. *Chem. Sci.* **2018**, *9*, 1551–1559. [CrossRef] [PubMed]
35. Wang, X.; Gao, C.-Q.; Gao, Z.-Y.; Wu, B.-L.; Niu, Y.-Y. Synthesis, crystallographic and spectral studies of homochiral cobalt(II) and nickel(II) complexes of a new terpyridylaminoacid ligand. *J. Mol. Struct.* **2018**, *1157*, 355–363. [CrossRef]
36. Jouad, E.M.; Larcher, G.; Allain, M.; Riou, A.; Bouet, G.M.; Khan, M.A.; Do Thanh, X. Synthesis, structure and bi-ological activity of nickel (II) complexes of 5-methyl 2-furfural thiosemicarbazone. *J. Inorg. Biochem.* **2001**, *86*, 565–571. [CrossRef]
37. Dixon, N.E.; Gazzola, C.; Blakeley, R.L.; Zerner, B. Jack bean urease (EC 3.5. 1.5). Metalloenzyme. Simple biological role for nickel. *J. Am. Chem. Soc.* **1975**, *97*, 4131–4133. [CrossRef]

38. Raj, P.; Singh, A.; Singh, A.; Singh, N. Syntheses and photophysical properties of Schiff base Ni(II) complexes: Application for sustainable antibacterial activity and cytotoxicity. *A.C.S. Sustain. Chem. Eng.* **2017**, *5*, 6070–6080. [CrossRef]
39. Kasuga, N.C.; Sekino, K.; Koumo, C.; Shimada, N.; Ishikawa, M.; Nomiya, K. Synthesis, structural characterization and antimicrobial activities of 4-and 6-coordinate nickel (II) complexes with three thiosemicarbazones and semicarbazone ligands. *J. Inorg. Biochem.* **2001**, *84*, 55–65. [CrossRef]
40. Kurtaran, R.; Yıldırım, L.T.; Azaz, A.D.; Namli, H.; Atakol, O. Synthesis, characterization, crystal structure and biological activity of a novel heterotetranuclear complex: [NiLPb (SCN) 2 (DMF)(H2O)] 2, bis-{[μ-N, N′-bis (sali-cylidene)-1, 3-propanediaminato-aqua-nickel(II)](thiocyanato)(μ-thiocyanato)(μ-N,N′ dimethylformamide) lead (II)}. *J. Inorg. Biochem.* **2005**, *99*, 1937–1944.
41. Kasuga, N.C.; Ohashi, A.; Koumo, C.; Uesugi, J.; Oda, M.; Nomiya, K. Synthesis, Structural Characterization, and Biological Activity of Two Different Nickel (II) Complexes Derived from N′-[1-(2-pyridyl) ethylidene] morpho-line-4-carbothiohydrazide. *Chem. Lett.* **1997**, *26*, 609–610. [CrossRef]
42. Oladipo, S.D.; Omondi, B.; Mocktar, C. Synthesis and structural studies of nickel (II)-and copper (II)-N, N′-diarylformamidine dithiocarbamate complexes as antimicrobial and antioxidant agents. *Polyhedron* **2019**, *170*, 712–722. [CrossRef]
43. Alexiou, M.; Tsivikas, I.; Dendrinou-Samara, C.; Pantazaki, A.A.; Trikalitis, P.; Lalioti, N.; Kyriakidis, D.A.; Kessissoglou, D.P. High nuclearity nickel compounds with three, four or five metal atoms showing antibacterial activity. *J. Inorg. Biochem.* **2003**, *93*, 256–264. [CrossRef] [PubMed]
44. Skyrianou, K.C.; Efthimiadou, E.K.; Psycharis, V.; Terzis, A.; Kessissoglou, D.P.; Psomas, G. Nickel–quinolones interaction. Part 1–Nickel (II) complexes with the antibacterial drug sparfloxacin: Structure and biological properties. *J. Inorg. Biochem.* **2009**, *103*, 1617–1625. [CrossRef] [PubMed]
45. Fathalla, E.M.; Abu-Youssef, M.A.M.; Sharaf, M.M.; El-Faham, A.; Barakat, A.; Badr, A.M.A.; Soliman, S.M.; Slawin, A.M.Z.; Woollins, J.D. Synthesis, Characterizations, Antitumor and Antimicrobial Evaluations of Novel Mn(II) and Cu(II) Complexes with NNN-tridentate s-Triazine-Schiff base Ligand. *Inorg. Chim. Acta* **2023**, 121586. [CrossRef]
46. Wang, L.; Wei, Z.L.; Chen, Z.Z.; Liu, C.; Dong, W.K.; Ding, Y.J. A chemical probe capable for fluorescent and colorimetric detection to Cu2+ and CN− based on coordination and nucleophilic addition mechanism. *Microchem. J.* **2020**, *155*, 104801. [CrossRef]
47. Wang, L.; Pan, Y.-Q.; Wang, J.-F.; Zhang, Y.; Ding, Y.-J. A highly selective and sensitive half-salamo-based fluorescent chemosensor for sequential detection of Pb(II) ion and Cys. *J. Photochem. Photobiol. A Chem.* **2020**, *400*, 112719. [CrossRef]
48. Sherif, O.E.; Abdel-Kader, N.S. DFT calculations, spectroscopic studies, thermal analysis and biological activity of supramolecular Schiff base complexes. *Arab. J. Chem.* **2018**, *11*, 700–713. [CrossRef]
49. Otwinowski, Z.; Minor, W. Processing of X-ray diffraction data collected in oscillation mode. *Methods Enzymol.* **1997**, *276*, 307–326. [PubMed]
50. *Rigaku Oxford Diffraction, CrysAlisPro*; Agilent Technologies Inc.: Oxfordshire, UK, 2020.
51. Sheldrick, G.M. Shelxt–integrated space-group and crystal-structure determination. *Acta Cryst.* **2015**, *A71*, 3–8. [CrossRef]
52. Sheldrick, G.M. *SADABS-Bruker Nonius Scaling and Absorption Correction-*; Bruker AXS Inc.: Madison, WI, USA, 2012.
53. Sheldrick, G.M. Crystal structure refinement with *SHELXL*. *Acta Crystallogr. Sect. C Struct. Chem.* **2015**, *71*, 3–8. [CrossRef] [PubMed]
54. Hübschle, C.B.; Sheldrick, G.M.; Dittrich, B. ShelXle: A Qt graphical user interface for SHELXL. *J. Appl. Crystallogr.* **2011**, *44*, 1281–1284. [CrossRef] [PubMed]
55. Spackman, M.A.; Jayatilaka, D. Hirshfeld Surface Analysis. *Cryst. Eng. Comm.* **2009**, *11*, 19–32. [CrossRef]
56. Lu, P.-L.; Liu, Y.-C.; Toh, H.-S.; Lee, Y.-L.; Liu, Y.-M.; Ho, C.-M.; Huang, C.-C.; Liu, C.-E.; Ko, W.-C.; Wang, J.-H. Epidemiology and antimicrobial susceptibility profiles of Gram-negative bacteria causing urinary tract infections in the Asia-Pacific region: 2009–2010 results from the Study for Monitoring Antimicrobial Resistance Trends (SMART). *Int. J. Antimicrob. Agents* **2012**, *40*, S37–S43. [CrossRef] [PubMed]